DOI: http://dx.doi.org/10.1590/1678-992X-2018-0349

ISSN 1678-992X

SCIENTIA AGRICOLA

Research Article

Repeated geophysical measurements in dry and wet soil conditions to describe soil water content variability

Daniela De Benedetto[1]*, Francesco Montemurro[2], Mariangela Diacono[1]

[1]Council for Agricultural Research and Economics/Research Centre for Agriculture and Environment, 5 – 70125 – Bari – Italy.

[2]Council for Agricultural Research and Economics/Research Centre for Vegetable and Ornamental Crops – 63077 – Monsampolo del Tronto (AP) – Italy.

*Corresponding author <daniela.debenedetto@crea.gov.it>

Edited by: Silvia del Carmen Imhoff

Received October 24, 2018

Accepted February 25, 2019

ABSTRACT: There is an increasing interest in the application of geophysical surveys to assess the soil water content (SWC) variation in both spatial and temporal scales. In this work, a geophysical survey was carried out at an experimental farm in dry and wet conditions. We determined the SWC data measured with the gravimetric method, apparent electrical conductivity by electromagnetic induction (EMI) and amplitude of Ground Penetrating Radar (GPR) data at different frequencies. Geophysical sensors are an efficient tool for soil mapping at high resolution; however; there is a need to improve the knowledge on their capabilities and limitations under field conditions, especially for GPR. The geophysical survey provides an example of the application of these techniques to evaluate the spatial variability of SWC in two different water conditions. The contribution of geophysical data in understanding the spatial variability of SWC was investigated applying both the traditional analysis and spatial techniques. The results indicated that the geophysical data captured the spatial variation of SWC in non-invasively way especially in dry condition. However, they also showed the complex interplay between factors controlling SWC and geophysical responses and the drawbacks of geophysical sensors under inhomogeneous water conditions. Our findings also highlighted that EMI survey provides the potential to map the SWC variability within a relatively short time. The results obtained in this research are important from the agronomical viewpoint, since they allow increasing efficiency of irrigation practices, which is important in times characterized by climate change.

Keywords: electromagnetic induction, ground penetrating radar, spatial and temporal variability, cross correlogram

Introduction

Soil water content (SWC) is a key component of the hydrological cycle, since it controls evapotranspiration, groundwater recharge and generation of runoff (Vereecken et al., 2014). Understanding the variation of SWC is important for the management of agricultural fields to maximize yields, apply irrigation systems and minimize the impacts of farming practices (Brocca et al., 2009). Investigation of the spatial pattern of SWC is having more attention with the increase in the availability of non-invasive soil sensors that integrate sparse direct sampling (Landrum et al., 2015). Geophysical sensors, such as electromagnetic induction (EMI) and ground penetrating radar (GPR), are gaining interest as tools to obtain spatially distributed data that could be correlated with soil and hydrologic properties (Zhu et al., 2010; Minet et al., 2013). The EMI methods are widely used for soil mapping, given the high density "on-the-go" surveys of soil apparent electrical conductivity (EC_a) (Adamchuk et al., 2004). EMI studies have been conducted to estimate the spatial variability of SWC (Martínez et al., 2010; De Benedetto et al., 2013) and it seems that the method allows mapping the soil properties with high spatial resolution (Martini et al., 2017; Pedrera-Parrilla et al., 2017). Time-lapse EMI measurements allow separation of the temporally stable contribution of static properties (e.g. texture) from the temporally dynamic contributions of SWC to the measured EC_a (Robinson et al., 2009). Conversely, research on GPR amplitude data is limited due to the complexity of data acquisition and processing. However, its application might provide important information because GPR data are sensitive to both soil EC and dielectric permittivity, primarily depending on SWC. GPR amplitude and measurements repeated in different water conditions could provide information on highly dynamic soil properties (Knight et al., 1997; De Benedetto et al., 2013). Although these technologies have potential to indicate features that influence the water movement, there is a need to further the knowledge on their capabilities and limitations under field conditions, especially for GPR applications. This study provides an example of geophysical application to evaluate GPR contribution in understanding the spatial variability of SWC in two different water conditions applying both the traditional analysis and spatial techniques, aimed at improving the use of EMI and GPR maps to describe spatial SWC patterns.

Materials and Methods

Study site and Data collection

The research was carried out at the experimental farm located in Metaponto (MT), southern Italy (lat. 40°24′ N; long. 16°48′ E; elev. 5 m asl). The study was conducted in the MITIORG experimental device (*Long-term climatic change adaptation in organic farming: synergistic combination of hydraulic arrangement, crop rotations, agro-ecological service crops and agronomic techniques*),

which consists of a long-term field trial in organic horticulture ongoing since 2013 and tests different agro-ecological techniques and conservation farming best practices (Diacono et al., 2016). The Soil, classified as Typic Epiaquerts (Soil Survey Staff, 1999), is poorly drained, consisting mostly of swelling clays, with the clay (about 60 %) and silt (30 %) contents increasing with depth.

The experimental device combines a suite of functionally integrated techniques from which the soil hydraulic arrangement obtained by means of soil surface shaping as a kind of ridge system, where different vegetable crops are cultivated both above three raised beds (ridges 2.5 m wide) and in four 2.5 m flat areas (or strips) between them (Figure 1A). This arrangement allows to increase the rooting depth layers in periods with high rainfall, eliminating the risk of water stagnation and making easier the lateral outflow of excess water (Diacono et al., 2016).

In July and October 2016, 36 geo-referenced soil samples were collected from the soil surface at 0.30 m depth at the four flat strips. The SWC was measured with gravimetric method. The samples were georeferenced using a Differential Global Positioning System (DGPS) with accuracy of altimetric and planimetric centimeter (Figure 1A). The dry conditions of July characterized the first data acquisition, whereas the Oct survey was characterized by large previous precipitation events (the last rainfall event occurred one week before the survey, about 21 mm). A Digital Elevation Model (DEM) was previously constructed (Figure 1B) and the elevation ranged from about 4 to 5 m above sea level (De Benedetto et al., 2017).

Geophysical investigations

The experimental field was surveyed using an EMI sensor connected to the DGPS. The system is composed of two units mounted perpendicularly to each other, which allows simultaneous measurements of EC_a at two depths for each measurement site. In the vertical dipole mode (V), the theoretical maximum sensitivity and investigation correspond to the depth of 0.40 and 1.50 m, respectively. In the horizontal dipole mode (H), device sensitivity decreases at depth to a theoretical maximum depth of investigation of 0.75 m (McNeill, 1980). The survey was conducted using a non-metallic platform and a wood cover (to avoid any magnetic interference and thermal drift of the sensor) and the sensor was towed behind a tractor at a distance of about 5 m, along 8 parallel longitudinal transects (approximately 1.5 m apart in each strip) (Figure 1A). The EMI sensor was calibrated and zeroed according to the manufacturer instruction before starting the measurements. The EC_a in both orientations (EC_a-H and EC_a-V) was recorded every second, resulting in an average spatial resolution of 0.5m along the transect.

The GPR survey was carried out immediately after the EMI survey, along 4 parallel longitudinal transects, about 8 m apart (Figure 1A). The GPR data were collected using a Multifrequency Array Radar-System, with two frequencies of antennas of 600 and 1600 MHz, operating in mono-static way. The GPR produces a short-pulse of high-frequency (10-1000 MHz) electromagnetic energy, which is transmitted into the ground. The propagation of the radar signal depends on the electrical properties of soil and are primarily controlled by the water content. Variations in the electrical properties of soils are usually associated to changes in volumetric water content, which, in turn, originates radar reflections (Davis and Annan, 1989). The GPR data were collected with trace increments of 0.024 m and time increments of 0.05 ns and connected with DGPS. The received signals were displayed as a function of their two-way travel in the form of radargram (Davis and Annan, 1989).

Statistical analyses

Descriptive statistical analyses were calculated and used to evaluate the magnitude of data dispersion. Since the condition of normality, checked by the Shapiro normality test, was not fulfilled, a non-parametric test,

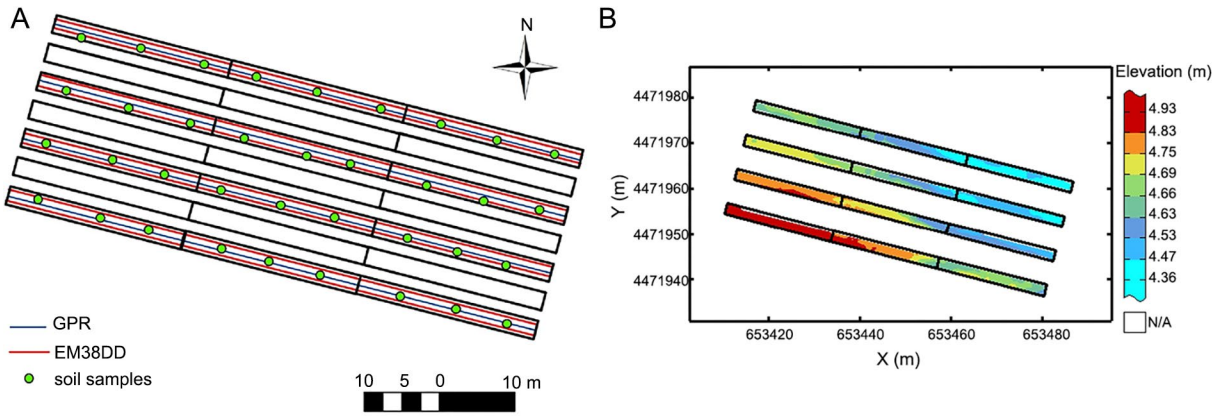

Figure 1 – (A) The experimental device with the sampling locations (green dots) and the EMI and GPR acquisitions (red and blue lines, respectively); (B) Spatial estimates of DGPS height.

Spearman's rank correlation coefficient, was calculated to correlate the variables at different times and their relationship to other soil properties. The statistical analyses of data were performed using the software package XLSTAT (Addinsoft SARL, Paris, France).

Pre-processing of geophysical data

The preliminary data analysis included both quality check and cleaning procedure. For EMI data, it is important to remove any points where the instrument was stationary. Any negative values were removed.

In this study, the processing of GPR data consisted of extracting quantifiable variables, such as attenuation and displaying GPR data in horizontal maps at a specified time (or depth). The pre-processing of GPR signal amplitude data also included the following set of filters (De Benedetto et al., 2015): static correction, dewow filter and trapezoidal bandpass filter and, finally, the instantaneous amplitude or envelope of data was calculated using a quadrature filter (Hilbert transformation). After that, the GPR data were reduced with a compression filter in distance–direction with an increment of 1 m. Amplitude maps (time slices) were built averaging the amplitude of the radar signal within a range of Δt width equal to the order of the dominant period of the antennas (2 ns and 1 ns for 600 and 1600 MHz antennas, respectively) by increasing time intervals up to 10 ns (about 0.5 m depth) and 5.5 ns (0.25 m depth) for 600 and 1600 MHz antennas, respectively. A mean velocity of 0.1 m ns^{-1} was calculated by means of the analysis of hyperbolae and the depth intervals were 0.1 m and 0.05 m for the both frequencies used. The data pre-processing was performed with ReflexW Software (Sandmeier Scientific Software, 2012).

Temporal variability analysis

In this study, the temporal persistence of a spatial pattern was investigated using the traditional time stability analysis, which consists in the computation of mean and standard deviation over time of the relative differences in SWC (Vachaud et al., 1985). The mean relative difference in soil water content $\overline{\delta}_{SWC}$ and the standard deviation of the relative differences $\sigma(\delta_{SWC})$ are given by:

$$\overline{\delta}_{SWC} = \frac{1}{n_t}\sum_{t=1}^{n_t}\frac{\theta_{i,t}-\overline{\theta}_t}{\overline{\theta}_t};$$

$$\sigma\left(\delta_{SWC}\right) = \sqrt{\frac{1}{n_t-1}\sum_{t=1}^{n_t}\left(\frac{\theta_{i,t}-\overline{\theta}_t}{\overline{\theta}_t}-\overline{\delta}_{SWC}\right)^2}$$

where n_t is the number of dates and $\overline{\theta}_t$ the spatial average of soil water content $\theta_{i,t}$ computed as follows:

$$\overline{\theta}_t = \frac{1}{n_i}\sum_{i=1}^{n_i}\overline{\theta}_{i,t}$$

where n_i is the number of locations within the field where the data were interpolated. The negative or positive values for the mean suggested that the variable measured both at a location and a specific date was always smaller (or greater) than the spatial mean obtained on the same date. The standard deviation of the relative difference $\sigma(\delta_{SWC})$ gives its degree of variation. The temporally stable locations should have the mean relative difference close to zero and with the minimum associated standard deviations (Martínez-Fernández and Ceballos, 2005; Coppola et al., 2011). An important insight can be derived by considering the spatial distribution of mean and standard deviation. Therefore, these outcomes were spatially displayed in raster format (0.5 × 0.5-m grid). The same calculations were applied to EMI and GPR data.

Mapping data using Geostatistics

For each date, one SWC map was estimated from 36 data points by ordinary kriging (OK) method (Matheron, 1963) on 0.5 × 0.5-m grid. The experimental variograms were calculated and fitted using a linear model of coregionalization (LMCs) for EMI and GPR data for each measurement date. The fitting parameter, tested by using cross-validation and calculating mean error (ME) and mean squared standardized error (MSSE) within a typical used tolerance of $1 \pm 3\mathrm{Sqrt}(2/N)$ (where N is the number of observations), were used to interpolate the data on the same grid using ordinary cokriging (CK) (Goovaerts, 1997). Even if ordinary kriging and cokriging did not require the data to follow a normal distribution, variogram modelling is sensitive to strong departures from normality, because a few exceptionally large values may contribute to very large squared differences. Therefore, all variables were transformed into Gaussian-shaped variables through a procedure known as Gaussian anamorphosis (Wackernagel, 2003). The Gaussian estimates were transformed back to the raw values through the Gaussian Anamorphosis model. All geostatistical analyses were performed with ISATIS software (Geovariances, 2015).

Cross correlogram

A geostatistical tool named cross-correlogram was used, which evaluates the strength of the relationship between two variables (A and B) as a function of spatial increment or lag ($\boldsymbol{h}$) separation. The cross-correlogram is calculated as:

$$r_c(\boldsymbol{h}) = \frac{\mathrm{cov}\left[A_i(x_i), B_i(x_i+\boldsymbol{h})\right]}{\sqrt{\mathrm{var}\left[A_i(x_i)\right]}\sqrt{\mathrm{var}\left[B_i(x_i+\boldsymbol{h})\right]}}$$

where i indicates the observation at location x_i (Webster and Oliver, 2001). It allows to examine the spatial aspects of the relationships, such as the range of distances over which the correlation between studied variables exists and the direction in space of the strongest and weakest correlation (Kravchenko et al., 2003). At zero distance, cross-correlogram is equal to the Pearson correlation coefficient, and at any $\mathbf{h} \neq 0$, cross-correlogram values depend on the direction of $\mathbf{h}$.

The cross-correlogram analysis was applied to measure the spatial correlation of all variables (SWC, EMI and GPR data) between two consecutive time steps (De Lannoy et al., 2006). Time stability is determined by studying the apex of the cross correlogram between two time steps. In particular, if the cross correlogram exhibits symmetry about the apex, the spatial distributions are consistent between time steps and the sources of variation remain stable with time. If, instead, it is not symmetric and shows the maximum or minimum at $\mathbf{h} = 0$, the presence of a delay means that the sources of variation for the two variables are not collocated, whereas the range informs the length of the natural influence of the variables.

Results and Discussion

Soil water content results

The SWC ranged between 11 and 17 % in July and between 15 and 20 % in Oct, showing drier conditions in the first survey compared to second one. A very small range of spatial variation coefficient (CV = 9.42 for July and CV = 8.45 for Oct) was observed, which could be attributed to the limited extension of the area as well as to the small heterogeneity of soil texture (Warrick and Nielsen, 1980). However, as reported by Brocca et al. (2009), the CV tended to be higher when the SWC decreased, denoting a larger soil moisture variability for drier conditions, as found in other studies (Famiglietti et al., 1999).

A variogram was fitted to the experimental variogram for each date of survey (Table 1). It is worth noting that fitted the variograms were quite similar for the two dates, with respect to the structures and sill variances, which is indicative of the consistence of the main spatial dependence over time. The greater sill variance was associated to wet condition, in Oct, than during dry periods, confirming the findings of Western et al. (1998). The relatively small range (R = 32 m), observed in the wettest condition, could be attributed both to a higher variable soil water distribution and lateral movement of water after precipitation events, which lead to shorter spatial correlation lengths of soil moisture (Western et al., 1998). In contrast, during period with less precipitation (July), the distribution of soil moisture was probably controlled by the differences in relatively stable properties (soil depth, texture and organic matter content) and, therefore, the spatial correlation length of the SWC was more localized and, thus, longer than for Oct (R = 60 m), (Zhu et al., 2010).

Both SWC maps estimated showed similar patterns with the wettest values located in the eastern part of the site as compared with the remaining part of it, where the driest values were observed (Figure 2). In the Oct map, the wettest SWC values were also encountered along the southern-western corner. However, the overall pattern of the SWC appeared visually similar, then, it was temporally stable. The part of the field with the highest SWC values corresponded mainly to lowest elevation values (Figure 1B) and there was a persistent wet area in this flat zone, although the slope is very gentle. The Spearman's rank correlation coefficient between elevation and SWC was negative for the July survey (-0.32 with $p < 0.0001$) and positive in Oct (0.08 with $p < 0.0001$). Since there were no changes in elevation in the experimental field between July and Oct, as shown in De Benedetto et al. (2017), the observed weak correlation between elevation and SWC may also be the outcome of combined effects of soil properties (Zhao et al., 2011). In any case, this persistent wet area reduced crop production, since the substantial presence of water during the cropping cycles affected negatively the main agronomical properties (Diacono et al., 2017).

Figure 3A presents the locations that were consistently higher and lower than the SWC average of the site. Persistently drier areas ($\overline{\delta}_{SWC}$)<0 or well drained areas were located in the central part of the site, whereas the wettest ($\overline{\delta}_{SWC}$)>0 areas were located in the southern-

Table 1 – Variograms fitted to the experimental variograms for SWC data in each survey. Mean error (ME) and mean standardized error (MSSE) are reported.

Date		Theorical variograms			Cross validation	
			Sill	Range	ME	MSSE
July	SWC	Nugget effect	0.380		0.068	1.03
		Spherical Model	0.990	60 m		
Oct	SWC	Nugget effect	0.096		0.015	1.05
		Spherical Model	1.107	32 m		

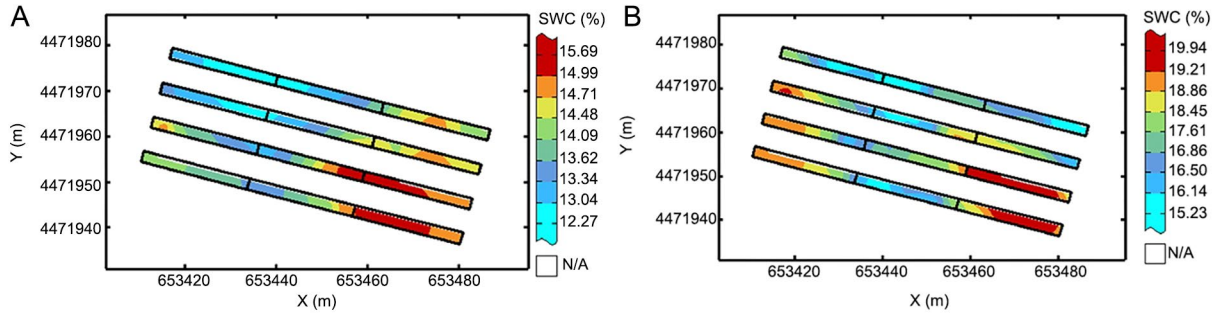

Figure 2 – Spatial estimates of gravimetric SWC in July (A) and in Oct (B) at 0-0.30 m depth. The color scale uses iso-frequency classes.

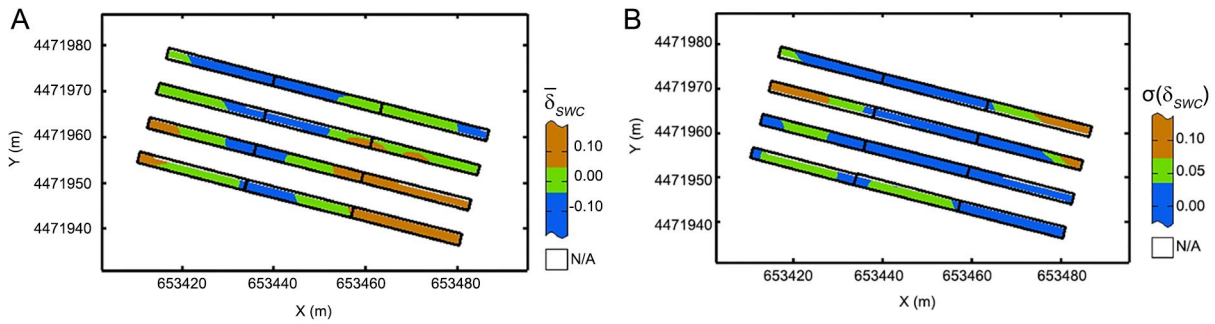

Figure 3 – Maps of the temporal stability: (A) the mean of relative difference of soil moisture to the field-average $\overline{\delta}_{SWC}$, (B) the standard deviation of the relative difference $\sigma(\delta_{SWC})$.

eastern border. In the eastern part of the field, there were both a depression and an increase of values from July to Oct, confirming the qualitative comments on the previous maps. The map in Figure 3B indicated the standard deviation over time of SWC differences to the field-average. The $\sigma(\delta_{SWC})$ values were very low indicating a high time-stability of soil moisture (Minet et al., 2013). However, slightly higher values were located in the western part and at northern-eastern border of the field. The areas with a major time variation were characterized by the highest and lowest elevation values, indicating that the variation between these two dates was likely, due to factors that influence the lateral and vertical distribution of water in the soil. This result is important from the agronomical point of view, since the knowledge of high time-stability of soil moisture and the variation of water distribution could support the choice of crops and the agronomical practices by the farmers, especially under climate change conditions (Diacono et al., 2016).

Figure 4 shows the cross-correlograms calculated for both consecutive surveys. The correlation coefficient at lag zero was high and positive (Pearson coefficient = 0.6), indicating moderate temporal autocorrelation (Landrum et al., 2016). The cross-correlogram was slightly asymmetric with the maximum value of correlation not centered at lag zero, indicating that the locations of the source of SWC variations were different from dry to wet conditions. This result could be due to the modifications in spatial structure (i.e. porosity). On the contrary, enough temporal persistence of spatial pattern might be more related mainly to soil texture. Since several factors influence the spatial variability of SWC, geophysical surveys could be used to interpret these results.

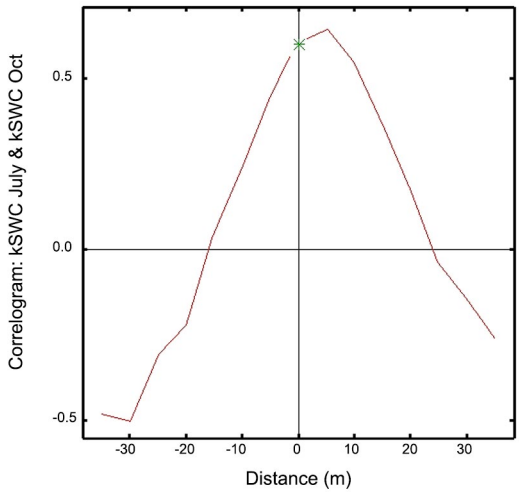

Figure 4 –The cross correlogram between estimates of SWC for July and Oct.

Soil apparent electrical conductivity maps

The EMI data are presented after removing the largest outlier point data because they were assumed not to be caused by real change of soil properties, but errors in data recording (Robinson et al., 2009). The mean EC_a values varied from 75.28 to 84.94 mS m^{-1} for EC_a-H and from 98.68 to 132.02 mS m^{-1} for EC_a-V, showing a small range of spatial variation. This result could be mainly attributed to the small variability of soil texture (Martini et al., 2017). The data recorded in Oct had lower means, standard deviations and CVs than in July, indicating a variability of EC_a between survey dates and, in particular, less variability in the Oct survey.

The two EMI variables were generally strongly correlated to each other for each survey date (Spearman correlation = 0.96 for July and 0.8 for Oct), suggesting homogeneity between shallow and deep horizons, although this correlation was partly due to deep EC_a integrating 1.5 m soil that includes the soil layer at 0.75 m (represented by EC_a-H). However, the correlation in Oct was lower, indicating either a possible soil discontinuity or an inhomogeneous water condition at soil depth. Although different authors have reported higher values of EC_a for wet surveys (Robinson et al., 2009; De Benedetto et al., 2013; De Caires et al., 2014), in this study, the statistics did not confirm these results. This could be at least partially attributed to transient conditions of soil water status after precipitation events.

The high correlation observed justified the use of a multivariate approach and, therefore, the linear models of coregionalization (LMCs) were fitted to the experimen-

tal variograms for each date, including the Nugget effect and Cubic model (R = 100 m) and the Nugget effect and Cubic model (R = 52 m) for July and Oct surveys, respectively. The different water conditions had not effects on the spatial structure of EC_a variograms, because the same model was fitted. The relative nugget effect was almost identical for both surveys, indicating that the unstructured portion of the total spatial variability (about 10 % of the total variance) was independent of the general soil moisture conditions. On the other hand, differences in the range were observed, as reported for the SWC variograms, showing a shorter range (R = 52 m) in the Oct survey and a longer one (about 100 m) in July. This last result suggests a control of the variable SWC on the EC_a variability (Zhu et al., 2010).

The maps of EC_a for each date (Figure 5) seemed to reveal a high level of spatial continuity along the soil profile, at least at ~1 m depth, because both EC_a maps were visually quite similar. All the maps showed an area with higher electrical conductivities in the western portion of the plot. The persistence of high values of EC_a in this part of the field over time might be attributed to intrinsic properties of the soil, such as textural and topographic characteristics, whereas the differences between the values of both EC_a variables were probably due to different moisture conditions at the soil/subsoil level (Brevik et al., 2006). This is confirmed by the Spearman's rank coefficient (0.78 and 0.60 for EC_a in vertical and horizontal polarizations between values collected in July and Oct, with $p < 0.0001$). Changes in EC_a-H were higher than in EC_a-V, since the main causes of variability occurred especially in the topsoil.

The maps of means of the difference of EC_a (Figures 6A and 6B) indicate a general increase in EC_a from the northern to the southern part of the field. The maps also showed that the values of $\overline{\delta}_{ECa}$ were close to zero for a large portion of the field. The range of $\overline{\delta}_{ECa}$ was more than twice the range of $\overline{\delta}_{SWC}$ since, not only SWC, but also other soil properties could influence EC_a (Pedrera-Parilla et al., 2017). These maps of temporal stability also suggest a general transition in soil texture, because of seasonal flooding in the study site, depositing the soil with fine texture along the field depression, as described in De Caires et al. (2014), and this was confirmed by soil sampling. This result suggests the need to restore periodically the soil hydraulic arrangement by means of soil surface shaping in the experimental device tested to allow crops cultivation also in the case of extreme climatic events. Moreover, the standard deviation of the temporal stability map for the EC_a measurements (Figures 6C and 6D) showed that the sites with greater changes were associated to the lowest part of the field, where water accumulated. Both maps exhibited similar spatial patterns, demonstrating that the EC_a patterns are independent from the depth of measurement, and these patterns could be used to map the study site (De Caires et al., 2014). Moreover, measurements of EC_a should be taken into account during the application of the usual agronomical practices.

Figure 7 shows the cross-correlograms of EC_a calculated for both consecutive surveys in both polarizations, allowing a more objective visual comparison between maps. The correlation coefficients at lag zero were high and positive (Pearson coefficients were 0.59 and 0.77 for horizontal and vertical polarizations, respectively), indicating moderate temporal autocorrelation. The cross-correlograms were slightly asymmetric with the maximum value of correlation not centered at lag zero, which suggests that the parameters driving conductivity variation were different on both dates. This is probably due to the interaction between SWC and other soil properties and

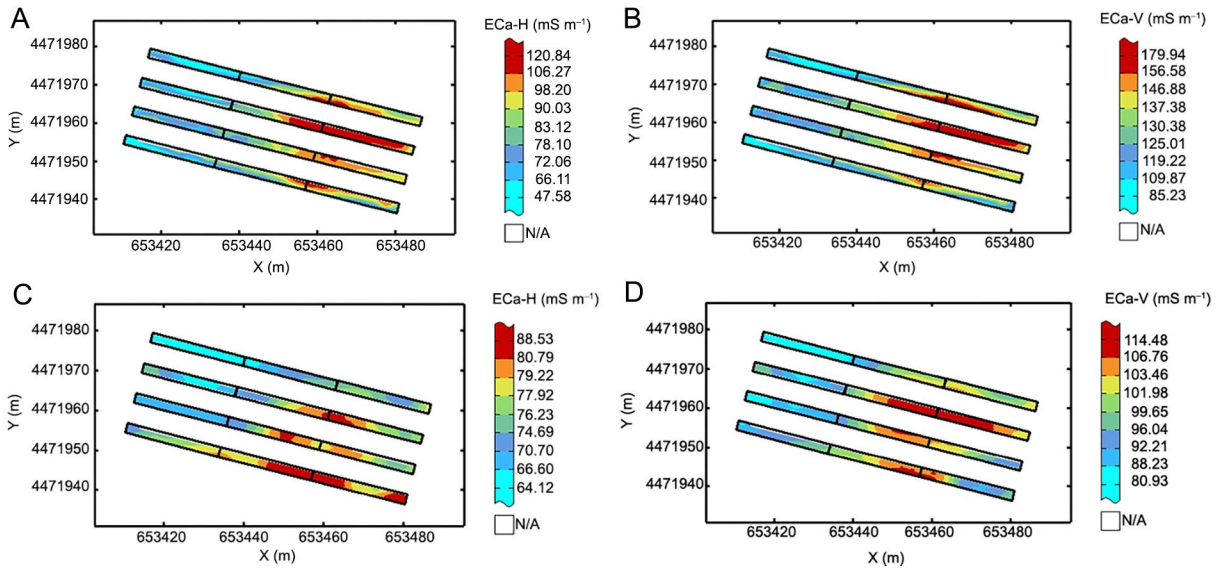

Figure 5 – Spatial estimates of EC_a in July survey in horizontal (A) and vertical (B) polarizations and in the Oct survey in horizontal (C) and vertical (D) polarizations, respectively. The color scale uses iso-frequency classes.

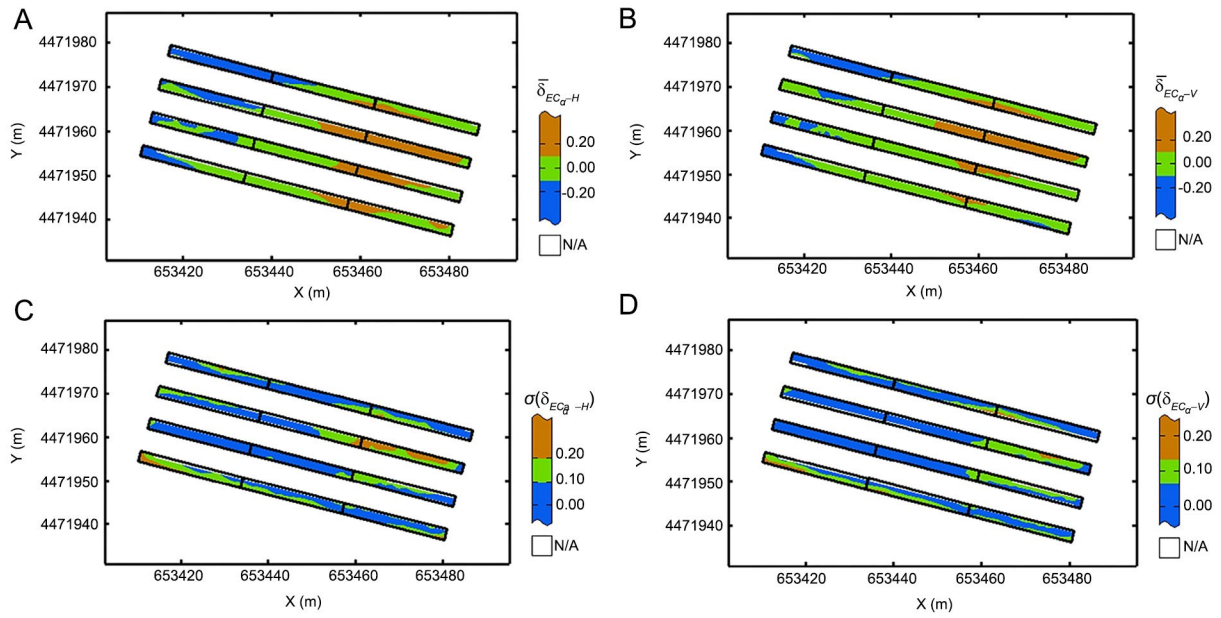

Figure 6 – Maps of temporal stability: (A and B) the mean of relative difference of ECa for field average in horizontal ($\overline{\delta}_{ECa\text{-}H}$) and vertical polarization ($\overline{\delta}_{ECa\text{-}V}$) respectively, (C and D) the standard deviation of relative difference in horizontal ($\sigma(\delta_{ECa\text{-}H})$) and vertical polarization ($\sigma(\delta_{ECa\text{-}H})$), respectively.

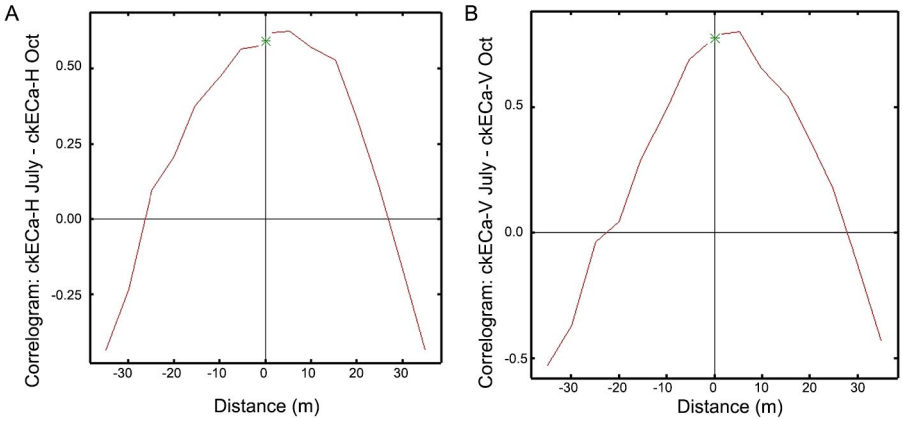

Figure 7 – The cross correlograms between the estimates of ECa for July and Oct in both horizontal (A) and vertical polarizations (B).

topography (Zhu et al., 2010; Martini et al., 2017). The cross-correlograms showed that the data were spatially associated within a range of about 25 m, which corresponded with the length of the cultivated sub-plots, indicating the average size of the area where EC_a values were high and low for different time steps.

The visual inspection of both estimated and temporal maps of EMI and SWC data showed remarkably similar spatial patterns, where the western end of the field had the highest EC_a and SWC values. However, the Spearman's rank coefficient (with $p < 0.0001$) for the July survey was 0.64 between EC_a-H and SWC and 0.52 between EC_a-V and SWC, proving that EMI data mostly reproduced the water patterns and confirming the homogeneity between shallow and deep horizons. On the other hand, for the Oct survey, a significant correlation with SWC was observed only for EC_a in horizontal polarization, but it was very low (0.34) and not clearly defined, confirming the results of previous studies where the correlation between EC_a and SWC was lower when the soil had higher moisture (Costa et al., 2014). One possible reason was the difference between the soil volume (0-0.30 m) explored by EMI measurements, which reflected a distribution of soil properties throughout the entire profile. However, the response of the EMI sensor in horizontal polarization is obtained from the soil volume about 0.50 m depth and thus the data related to horizontal polarization are at least partly influenced by values below 0.30 m in the experimental field. This result implied that variability of the moisture content did not significantly influ-

ence variability of EC_a and probably the correlation was higher with other soil properties or that the sources of variation changed at these two dates. Therefore, not only the surface topography, but also soil discontinuities, plays a significant role in influencing spatial EC_a variation thus confirming results of a previous work (De Benedetto et al., 2017). Since this type of sensor, which provides an integrated signal along the surveyed soil profile, is not capable of locating the discontinuity and displaying the vertical stratification, a GPR was used because its outcomes can be located in a 3D space.

Ground penetrating radar results

The amplitude maps, one of the most impressive ways of displaying GPR data, were created. The mean values of the GPR time slices (values not reported) showed a clear attenuation of the signal at depth, as expected. Since the data still showed some departure from the normal distribution even after the removal of outliers (points outside $\pm$ 2.5 standard deviations) and the hypothesis of normality was refused, these data were transformed into Gaussian scores and an LMC was fitted to all experimental direct and cross-variograms separately for each antenna.

The LMCs for 600 MHz antenna consisted of the following basic structures: (1) in the July survey: the Nugget effect, Spherical model (R = 10 m) and Spherical model (R = 33 m); (2) in the Oct survey: the Nugget effect, Spherical model (R = 8 m) and Spherical model (R = 33 m). Also for GPR, the different water condition had no effect on the fitted structures, suggesting consistence of the main spatial dependence over time. However, the spatial structures decomposed the total variance into three components: uncorrelated error (about 29 and 55 % for July and Oct, respectively), shorter-scale variance (about 46 and 15 % for July and Oct, respectively), longer-scale variance (about 25 and 30 % for July and Oct, respectively). The relative nugget effect was different for both surveys: in wet condition, the main component of variation was related to nugget variation, which can be ascribed to small variability of the scale and could be largely affected by error measurement. The processing of GPR data was identical for both surveys, suggesting that the unstructured portion of total spatial variability was dependent on the SWC. In particular, in the Oct survey, the spatial structures were not well defined, probably due to an increase of soil inhomogeneity produced by water along the vertical profile, contrary to what was described in De Benedetto et al. (2013).

The amplitude maps estimated for both surveys at the depths investigated did not display consistency along the profile at 0.30 m depth, due to variations of soil depth of different interfaces recognized based on the pre-existing pedological profile (Ventrella et al., 2000). Only the map related to time slice at 6 ns (0.30 m depth) was reported here. The map in July (Figure 8A) showed the same field division observed in the SWC and EMI maps, with a tendency towards low amplitude signals in the eastern part of the field, except for the third strip, due to the variations in soil depth (Ventrella et al., 2000). In particular, in the third strip, the area with higher values of amplitudes corresponded to higher EC_a values in both polarizations. This result might be due to a high degree of soil compaction, which reflected the radar signal and it retained water, indicating an increase in electrical conductivity. However, a relationship was calculated between SWC and GPR signals at 0.30 m depth in July and the correlation coefficient was negative (Spearman's rank coefficient = –0.22 with $p < 0.0001$), as expected.

In the Oct survey, all depth slices were different from slices observed in July survey, confirming the previous findings on spatial components. The absolute values of amplitude at 0.3 m depth were higher than in July map and the areas with high amplitude values, in the eastern portion of the field, corresponded to the areas with higher SWC and EC_a values (Figure 8B). In fact, the correlation coefficient was positive (Spearman's rank coefficient = 0.22 with $p < 0.0001$). In the wet condition, the GPR signal was less attenuate than in the dry condition, although, based on the physical principle, attenuation of the radar signal an increase as the soil water content rises. This is possibly because there is no direct and unique relationship between the GPR signal and SWC or water conditions were not homogenous and stable at the moment of the survey.

The LMCs for 1600 MHz antenna consisted of the following basic structures: (1) in the July survey: the Nugget effect, Spherical model (R = 9 m) and Spherical model (R = 33 m); (2) in the Oct survey: the Nugget effect, Spherical model (R = 10 m) and Spherical model (R = 45 m). The 1600 MHz variograms were typically noisier

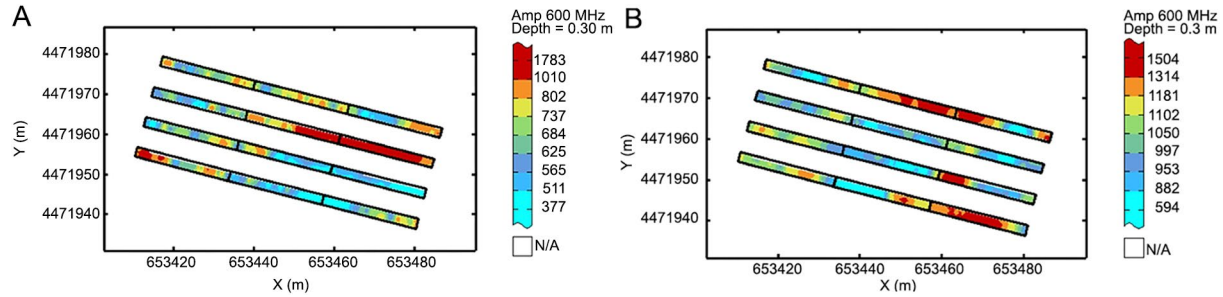

Figure 8 – Estimated amplitude maps for 600 MHz antenna at 0.30 m in July (A) and in Oct (B). The color scale uses iso-frequency classes.

compared with those for 600 MHz antenna because of their finer spatial resolution. The unstructured portion of the total spatial variability was very high in both water conditions (about 57 and 67 % for July and Oct, respectively) and the shorter-scale variance was about 21 and 17 % and longer-scale variance was about 22 and 16 % for July and Oct, respectively.

The map of the estimated amplitude for 1600 MHz antenna at 0.25 m depth for July (Figure 9A) showed low amplitude signals in the first two strips (southern part of the field) and a relative high amplitude in the last two strips. The situation was opposite in the Oct survey (Figure 9B). Therefore, the maps of the estimated amplitude for 1600 MHz antenna did not show similar spatial structures compared with those for 600 MHz antenna, because of its finer spatial resolution. These differences might be due to the different water conditions producing a variability in microstructures, as the GPR system for 600 MHz antenna did not detect because of their coarser spatial resolution.

However, the correlation between GPR data at 1600 MHz frequencies and SWC confirmed the positive correlation and, as a consequence, the higher values were observed in the dry condition.

The relationships between estimated amplitude in July and in Oct for both frequencies were calculated and the Spearman's rank coefficients were negative and low (–0.09 and –0.3 for 600 MHz and 1600 MHz antenna, respectively and with $p < 0.0001$). The maps of temporal stability (Figures 10A and 10B) indicated a general decrease in amplitude values for 600 MHz antenna in the western part of the field and showed that a large portion of the field had values close to zero for 1600 MHz antenna. The ranges of $\overline{\delta}_{Amp\_}$ for both frequencies were greater than the range of $\overline{\delta}_{SWC}$ and $\overline{\delta}_{ECa}$, suggesting that the amplitude was probably influenced by different soil properties. The standard deviation of the temporal stability maps (Figures 10C and 10D) showed the areas with greater changes in the western part of the field, where water distribution and EMI measurements were

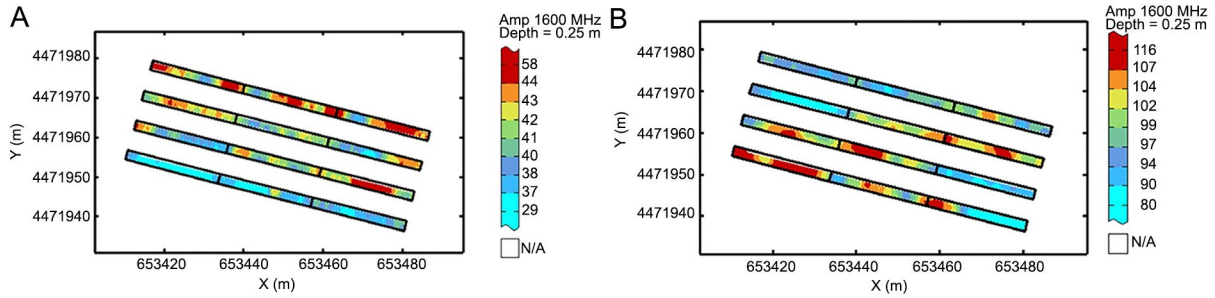

Figure 9 – Estimated amplitude maps for 1600 MHz antenna at 0.25 m in July (A) and in Oct (B). The color scale uses iso-frequency classes.

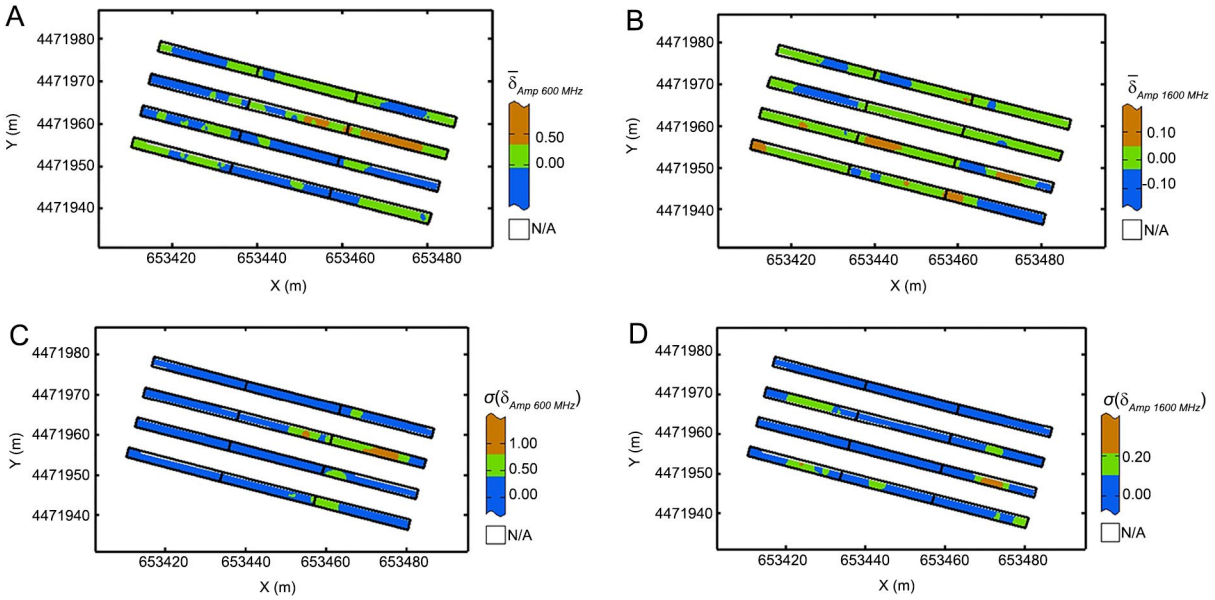

Figure 10 – Maps of the temporal stability: (A and B) the mean of relative difference of amplitude (Amp) for field average for 600 MHz ($\overline{\delta}_{Amp600MHz}$) and 1600 MHz ($\overline{\delta}_{Amp1600MHz}$) frequencies, (C and D) the standard deviation of relative difference for 600 MHz ($\sigma(\delta_{Amp600\ MHz})$) and 1600 MHz ($\sigma(\delta_{Amp1600\ MHz})$) frequencies.

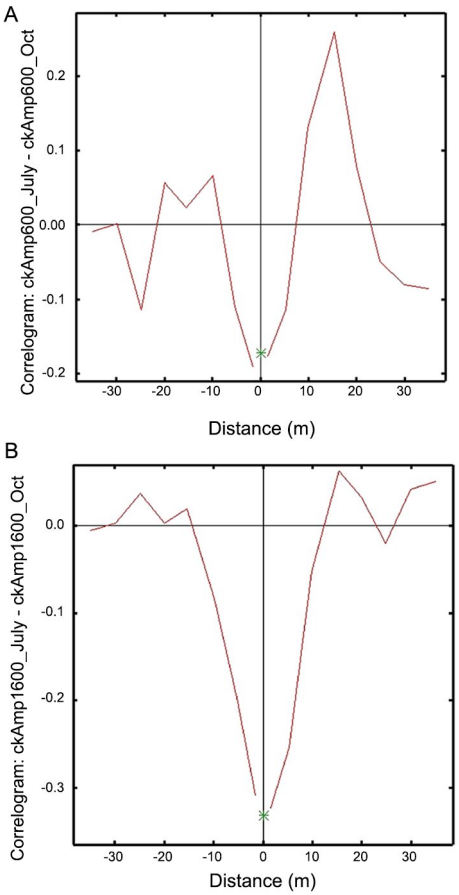

Figure 11 – The cross correlograms between estimates of amplitude for July and Oct for 600 MHz (A) and 1600 MHz (B) frequencies.

also subjected to change in time. Although the standard deviation of maps for temporal stability showed that the most field was stable in these consecutive time steps, the cross-correlograms (Figure 11) indicated that the relationships at lag zero were negative and asymmetric revealing that variation sources for the GPR signal were shifted in this time step, probably due to transitory interaction, which spatially influenced the GPR signal. This geostatistical tool added spatial information to the correlation coefficient calculated and the approach of Vauchad et al. Finally, the analysis of GPR data showed that SWC variability is best characterized using measurements obtained when the soil is dry.

Conclusions

The geophysical surveys conducted in two different water conditions allowed to study the effects of SWC on geophysical data (EC_a and GPR amplitude). Although the range of SWC variations was not large and the results showed a moderate time-stability, differences in EMI and GPR responses were observed. Moreover, this study proved that the integrating traditional approach (method of Vachaud et al.) and the geostatistical analysis allow deeper understanding into the soil moisture patterns throughout time. The cross-correlogram is an effective approach to study time stability and provide information on sources of soil water variation, particularly during a transitioning stage between soil wetting and drying phases. These findings are important in agriculture, since they help to maximize crop yield, increase efficiency of irrigation systems and minimize potential environmental effects of agricultural practices, especially during the current period characterized by climate change. The results showed that the soil moisture was not the only variable that influenced geophysical data. Therefore, in order to improve the correlation between SWC and geophysical values, the water condition should be as homogenous as possible within the study site to allow understanding and predicting soil moisture variation, which is important for farming activities. These findings justify the need for further research with repeated measurements over multiple wetting and drying cycles to clarify the relationship between these variables and understand long–term time stable characteristics of SWC.

The results obtained in this work also support the conclusion that EMI survey, much more than GPR, presents potential to map the SWC variability, non-invasively and with high spatial resolution, and to capture dynamic changes in soil moisture. However, to the best of our knowledge, there are no studies using temporal stability characteristics revealed by GPR surveys to investigate the temporal stability pattern of SWC. These results confirm the advantages of using different proximal sensors as a preliminary step for several agricultural applications where knowledge on the spatial distributions of SWC is critical. These results should be thus verified by conducting field acquisitions over larger areas, for different topographies and surface conditions.

Acknowledgements

This paper is a result of the AGROCAMBIO (Sistemi e tecniche AGROnomiche di adattamento ai CAMbiamenti climatici in sistemi agricoli BIOlogici) and RETIBIO (Attività di supporto nel settore dell'agricoltura biologica per il mantenimento dei dispositivi sperimentali di lungo termine e il rafforzamento delle reti di relazioni esistenti a livello nazionale e internazionale) research projects funded by the Organic Farming Office of the Italian Ministry of Agriculture.

Authors' Contributions

Conceptualization: De Benedetto, D.; Montemurro, F.; Diacono, D. Data acquisition: De Benedetto, D.; Montemurro, F.; Diacono, D. Data analysis: De Benedetto, D. Design of methodology: De Benedetto, D.; Montemurro, F.; Diacono, D. Writing and editing: De Benedetto, D.; Montemurro, F.; Diacono, D.

References

Adamchuk, V.I.; Hummel, J.W.; Morgan, M.T.; Upadhyaya, S.K. 2004. On-the-go soil sensors for precision agriculture. Computers and Electronics in Agriculture 44: 71–91.

Brevik, E.; Fenton, T.; Lazari, A. 2006. Soil electrical conductivity as a function of soil water content and implications for soil mapping. Precision Agriculture 7: 393-404.

Brocca, L.; Melone, F.; Moramarco, T.; Morbidelli, R. 2009. Soil moisture temporal stability over experimental areas in Central Italy. Geoderma 148: 364–374.

Coppola, A.; Comegna, A.; Dragonetti, G.; Lamaddalena, N.; Kader, A.M.; Comegna, V. 2011. Average moisture saturation effects on temporal stability of soil water spatial distribution at field scale. Soil and Tillage Research 114: 155–164.

Costa, M.M.; Queiroz, D.M.; Carvalho Pinto, F.A.; Reis, E.F.; Santos, N.T. 2014. Moisture content effect in the relationship between apparent electrical conductivity and soil attributes. Acta Scientiarum. Agronomy 36: 395-401.

Davis, J.L.; Annan, A.P. 1989. Ground-penetrating radar for high-resolution mapping of soil and rock stratigraphy. Geophysical Prospecting 37: 531-551.

De Caires, S.A.; Wuddivira, M.N.; Bekele, I. 2014. Assessing the temporal stability of spatial patterns of soil apparent electrical conductivity using geophysical methods. International Agrophysics 28: 423-433.

De Benedetto, D.; Castrignanò, A.; Quarto, R. 2013. A geostatistical approach to estimate soil moisture as a function of geophysical data and soil attributes. Procedia Environmental Sciences 19: 436 – 445.

De Benedetto, D.; Quarto, R.; Castrignanò, A.; Palumbo, D.A. 2015. Impact of data processing and antenna frequency on spatial structure modelling of GPR data. Sensors 15: 16430-16447.

De Benedetto, D.; Montemurro, F.; Diacono, M. 2017. Impacts of agro-ecological practices on soil losses and cash crop yield. Agriculture 7: 103.

De Lannoy, G.; Verhoest, N.; Houser, P.; Gish, T.; Meirvenne, M. 2006. Spatial and temporal characteristics of soil moisture in an intensively monitored agricultural field (OPE^3). Journal of Hydrology 331: 719-730.

Diacono, M.; Fiore, A.; Farina, R.; Canali, S.; Di Bene, C.; Testani, E.; Montemurro, F. 2016. Combined agro-ecological strategies for adaptation of organic horticultural systems to climate change in Mediterranean environment. Italian Journal of Agronomy 11: 730: 85- 91.

Diacono, M.; Persiani, A.; Fiore, A.; Montemurro, F.; Canali, S. 2017. Agro-ecology for adaptation of horticultural systems to climate change: agronomic and energetic performance evaluation. Agronomy 7: 35.

Famiglietti, J.S.; Devereaux, J.A.; Laymon, C.A.; Tsegaye, T.; Houser, P.R.; Jackson, T.J.; Graham, S.T.; Rodell, M.; van Oevelen, P.J. 1999. Ground-based investigation of soil moisture variability within remote sensing footprints during the Southern Great Plains 1997(SGP97) Hydrology Experiment. Water Resources Research 35: 1839–1851.

Goovaerts, P. 1997. Geostatistics for Natural Resources Evaluation. Oxford University Press, Oxford, UK. (Applied Geostatistics Series).

Knight, R.; Tercier, P.; Jol, H. 1997. The role of ground-penetrating radar and geostatistics in reservoir description. The Leading Edge 16: 1576–1582.

Kravchenko, A.N.; Thelen, K.D.; Bullock, D.G.; Miller, N.R. 2003. Relationship among crop grain yield, topography, and soil electrical conductivity studied with cross-correlograms. Agronomy Journal 95: 1132–1139.

Landrum, C.; Castrignanò, A.; Mueller, T.; Zourarakis, D.; Zhu, J.; De Benedetto, D. 2015. An approach for delineating homogeneous within-field zones using proximal sensing and multivariate geostatistics. Agricultural Water Management 147: 144-153.

Landrum, C.; Castrignanò, A.; Zourarakis, D.; Mueller, T. 2016. Assessing the time stability of soil moisture patterns using statistical and geostatistical approaches. Agricultural Water Management 177: 118-127.

Martínez, G.; Vanderlinden, K.; Giráldez, J.V.; Espejo, A.J.; Muriel, J.L. 2010. Field scale soil moisture pattern mapping using electromagnetic induction. Vadose Zone Journal 9: 871.

Martínez-Fernández, J.; Ceballos, A. 2005. Mean soil moisture estimation using temporal stability analysis. Journal of Hydrology 312: 28–38.

Martini, E.; Werban, U.; Zacharias, S.; Pohle, M.; Dietrich, P.; Wollschläger, U. 2017. Repeated electromagnetic induction measurements for mapping soil moisture at the field scale: validation with data from a wireless soil moisture monitoring network. Hydrology and Earth System Sciences 21: 495–513.

Matheron, G. 1963. Principles of geostatistics. Economic Geology 58: 1246-1266.

McNeill, J.D. 1980. Electromagnetic Terrain Conductivity Measurement at Low Induction Numbers. Geonics, Mississauga, Canada. (Technical Note, 6).

Minet, J.; Verhoest, N.E.C.; Lambot, S.; Vanclooster, M. 2013. Temporal stability of soil moisture patterns measured by proximal ground-penetrating radar. Hydrology and Earth System Sciences 10: 4063–4097.

Pedrera-Parrilla, A.; Pachepsky, Y.A.; Taguas, E.V.; Martos-Rosillo, S.; Giráldeze, J.V.; Vanderlinden, K. 2017. Concurrent temporal stability of the apparent electrical conductivity and soil water content. Journal of Hydrology 544: 319-326.

Robinson, D.A.; Lebron, I.; Kocar, B.; Phan, K.; Sampson, M.; Crook, N.; Fendorf, S. 2009. Time-lapse geophysical imaging of soil moisture dynamics in tropical deltaic soils: an aid to interpreting hydrological and geochemical processes. Water Resources Research 45: W00D32.

Soil Survey Staff. 1999. Soil Taxonomy. USDA-NRCS, Washington, DC, USA. (Agriculture Handbook, 436).

Vachaud, G.; De Silans, A.; Balabanis, P.; Vauclin, M. 1985. Temporal stability of spatially measured soil water probability density function. Soil Science Society of America Journal 49: 822–828.

Ventrella, D.; Mohanty, B.P.; Simunek, J.; Losavio, N.; van Genuchten, M.T. 2000. Water and chloride transport in a fine-textured soil: field experiments and modelling. Soil Science 165: 624-631.

Vereecken, H.; Huisman, J.A.; Pachepsky, Y.; Montzka, C.; van der Kruk, J.; Bogena, H.; Weihermüller, L.; Herbst, M.; Martinez, G.; Vanderborght, J. 2014. On the spatio-temporal dynamics of soil moisture at the field scale. Journal of Hydrology 516: 76–96.

Wackernagel, H. 2003. Multivariate Geostatistics: An Introduction with Applications. Springer, Berlin, Germany.

Warrick, A.W.; Nielsen, D.R. 1980.Spatial Variability of Soil Physical Properties in the Field. Academic Press, New York, NY, USA.

Webster, R.; Oliver, M.A. 2001. Geostatistics for Environmental Scientists. Wiley, Chichester, UK.

Western, A.W.; Blöschl, G.; Grayson, R.B. 1998. Geostatistical characterisation of soil moisture patterns in the Tarrawarra catchment. Journal of Hydrology 205: 20-37.

Zhao, Y.; Peth, S.; Hallett, P.; Wang, X.; Gi, M.; Gao, Y.; Horn, R. 2011. Factors controlling the spatial patterns of soil moisture in a grazed semi-arid steppe investigated by multivariate geostatistics. Ecohydrology 4: 92-104.

Zhu, Q.; Lin, H.; Doolittle, J. 2010. Repeated electromagnetic induction surveys for determining subsurface hydrologic dynamics in an agricultural landscape. Soil Science Society of America Journal 74: 1750–1762.